A practical example why anisotropy matters - A CSEM case study from South East Asia

Syarina Azura Mohamad*, Lars Lorenz, Lim Toon Hoong, Tan Kian Wei, EMGS Asia Pacific; Sandeep K. Chandola, Nurul Saadah, Fatma Nazihah, PETRONAS Carigali Sdn. Bhd.

Summary

A 3D CSEM survey was acquired in a frontier deepwater area in SE-Asia to provide input for portfolio ranking and risk mitigation. The interpretation process of the 3D data set was heavily driven by 3D inversion. Various 3D inversion approaches were tested and the results demonstrated the importance of including anisotropy.

Interpretations based on the isotropic 3D inversion differ from the interpretation of the anisotropic result, the latter coinciding with the pre-survey geomodel. The final interpretation of the CSEM data suggested significant hydrocarbon charge to be restricted to only one-third of the original prospect area, off the crest of the structure, reducing the potential of the prospect significantly.

Introduction

A 3D CSEM data set was acquired in 2008 in a deepwater acreage in SE Asia with water depth ranging from 1700 to 1900m. The survey was part of a portfolio ranking campaign to mitigate the drilling risk and associated costs for deepwater frontier exploration. The area is characterized by basement pop-ups, finding a structural expression up to the seafloor level.

The target of this survey is associated with one of these structures and characterized by internal faulting and possibly compartmentalization. Also, initial 3D CSEM modeling studies suggested that only moderate EM anomalies would be present. To increase the confidence in the interpretation, and to take into account the wide range of possible target area, a 3D survey geometry was employed. In addition, this survey geometry gives access to more advanced processing routines, in particular 3D inversion.

This paper presents the interpretation workflow applied to this dataset. It also outlines some of the challenges which may be encountered when treating a 3D data set in an oversimplified manner, especially with respect to the impact of anisotropy on the interpretation.

Methodology

The initial commercial application of CSEM for hydrocarbon exploration was introduced by Eidesmo et al. in 2002. An active source emits an electromagnetic field which diffuses in the subsurface and is attenuated in response to the resistivity distribution of the subsurface.

A receiver array records the attenuated signal at a varying distance from the source and the recorded data is analyzed to reconstruct the resistivity distribution in the subsurface. As hydrocarbon bearing sediments in clastic environments are characterized by resistivities up to two orders of magnitude higher than the water bearing sediments, this resistivity information can be used to de-risk and rank exploration prospects (Eidesmo et al., 2002).

First pass data analysis

The data processing follows the processing procedure as outlined by Zach et al. (2008). The initial data analysis was performed by using relative responses in form of a normalized magnitude versus offset (NMvO) and phase difference versus offset (PDvO). While this approach does not yield reliable depth information and struggles with complex settings, the short turn-around time aids in obtaining an overall impression of the complexity of the data set at a very early stage. It also provides indications of the accuracy of the initial model with respect to the complexity.

Figure 1 shows an NMvO response map at one of the acquired frequencies. Approximately one third of the prospect area shows stronger NMvO response than the reference area to SE, indicating higher resistivities in the NE region of the prospect. In addition, stronger responses are observed towards the SW, NE and NW of the survey area. These anomalies showed a clear correlation with the thickness variations of a shallow stratigraphic interval.
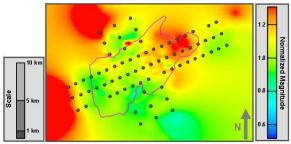

Figure 1: Normalized Magnitude versus Offset at 1.0 Hz and 5000m offset. Grey circles represent the receivers deployed and the red polygon shows the prospect outline.

Unconstrained 3D Inversion

The 3D inversion algorithm, described by Stoeren et al. (2008) and Zach et al. (2008), utilizes a quasi Newton optimization scheme. The inversion of the dataset was performed in several stages. The starting model was based on 1D inversion of receivers, interpolation between these resistivity traces and three-dimensional smoothing. This ensured a starting model with low initial misfit and no sharp resistivity boundaries, reducing the potential for inversion artifacts.

Initially, only an isotropic inversion was performed on the dataset. For the first run, only the inline data was inverted. A speed advantage is associated with the reduced data volume, and this approach would correspond to treating the data as a 2D grid survey. Figure 2 shows the result of the isotropic 3D inversion of the inline data for the six lines.

A highly resistive body is imaged, correlating well in extension with the previously indicated anomaly in the relative response. Nevertheless, interpretation of this inversion result could prove to be difficult as the vertical extension of the resistor is about 500 m. Such a poor resolution in depth makes it difficult to correlate the resistor to a specific seismic event.
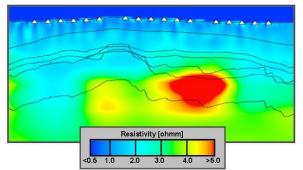

Figure 2: Isotropic 3D inversion result of inline data for all six lines.

To benefit from the advantage of a 3D data set which was outlined by Morten et al. (2009), a second run, including azimuth data, was performed. Significant improvements in the depth allocation of the resistor are achieved when including the azimuth data (Figure 3, top). The main resistor is much better focused vertically, improving its correlation with a seismic event. An additional weaker resistive event also starts to show-up at the original prospect level.

However, when analyzing the data misfit, it becomes apparent that the isotropic inversion result for the full 3D dataset only manages to explain the inline data to a

satisfactory degree, while the second component, the azimuth data, shows errors in excess of 50% (Figure 3, bottom). In addition, a meaningful geological interpretation of the high resistivities at this depth interval could not be achieved.
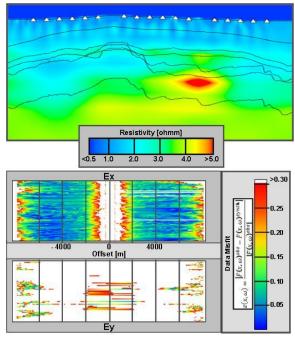

Figure 3: Isotorpic 3D inversion result for the full 3D data set (top) and the resulting misfit for the Ex and Ey component of the electric field (bottom).

Lu and Xia (2007) noted that the azimuth data has a high sensitivity to the horizontal resistivity. As this is not accounted for in the previous inversion runs, an anisotropic 3D inversion was performed to obtain a better match for the azimuthal data.

Figure 4 shows the result for the anisotropic 3D inversion of the full 3D dataset. A well-defined resistor is imaged, this time, correlating well with the anticipated target interval, imaged about 500 m shallower than in the isotropic 3D inversion result. Considering the data misfit for this inversion run, it can be clearly seen that placement of the resistor at the anticipated depth not only improves our ability to find a geological interpretation for the increased resistivities, but also our capability to match the azimuthal data.

From these inversion tests, it became evident that at the one hand, the treatment of the data set as a compilation of 2D lines may yield a result which is difficult to correlate to seismic events, and at the other hand, the full complexity

of the subsurface has to be taken into account to recover a resistivity model which explains the full 3D data set. These observations formed the basis of the final step, the integration of the CSEM data with the available seismic data.
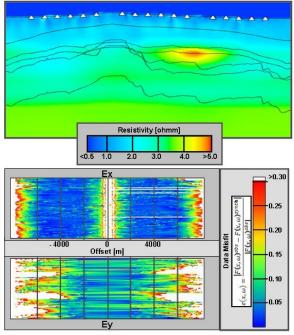

Figure 4: Anisotropic 3D inversion result (vertical resistivity) for the full 3D data set (top) and the resulting misfit for Ex and Ey component of the elctric field (bottom).
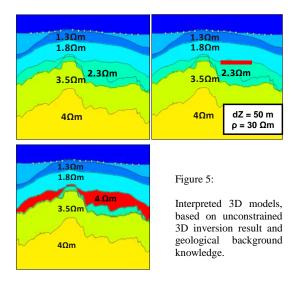
Data Integration

The final integration of the 3D inversion results was a combined 3D modeling and constrained 3D inversion study. The challenge for the area was the lack of hard resistivity data which could be fed directly into a constrained 3D inversion, either in form of well logs or in form of proven resistivity interfaces.

Geological interpretation on a regional scale was used to identify possible resistivity interfaces and 3D models were built to test these hypotheses. CSEM data exhibits the highest sensitivity to resistivity variations in the shallow section of the subsurface. Therefore, special care was taken for populating this part of the model and extensive 2.5D inversion tests were run for the high frequency data to derive the variability in resistivity for this section. Results of this 2.5D test showed a variability of less than 0.3 ohmm.

Figure 5 shows the derived background model (top left) and two of the interpreted models, accounting for the local

resistivity increase. The model with the best overall data misfit includes a thin resistor at the prospect level at the eastern flank of the structure (top right), but an alternative explanation in form of a high resistive sediment package, thickening significantly towards the eastern side, could be envisioned as well (bottom).

Figure 5:

Interpreted 3D models, based on unconstrained 3D inversion result and geological background knowledge.

To refine the interpretation model, a constrained anisotropic 3D inversion was performed. A strong bias towards the interpretation models would exist as they are used as base to define the resistivity interfaces. In addition to the fine-tuning of the interpretation model, it was aimed at obtaining additional indications for or against either of the two models with higher resistivities.

Updating for the shallow stratigraphic intervals above the target zone was restricted to a narrow band of resistivity values, derived from the high frequency 2.5D inversion tests which accounts for minor lithology changes. No resistivity limitations were placed on the interval at or below the target zone.

Figure 6 shows the constrained anisotropic 3D inversion result as well as the associated data misfit. The data misfit is slightly larger than the unconstrained result towards the edge of the survey area. This can be attributed to two different factors-the degree of freedom is reduced, not allowing for fine-tuning of the misfit anymore, and the seismic horizons are partially interpolated in this area.

The strength of the resistor is increased in comparison to the unconstrained inversion result. In addition, the main resistivity accumulation offset towards east by approximately 3 km. A weaker resistive accumulation is observed bridging the gap from the flank of the structure to the main accumulation. This resistivity distribution is more

in line with the thin resistor interpretation model (Figure 5, top right), than that with the thick resistive sequence model (Figure 5, bottom) and may be taken as an indication that the model with a reservoir type resistor is more likely.
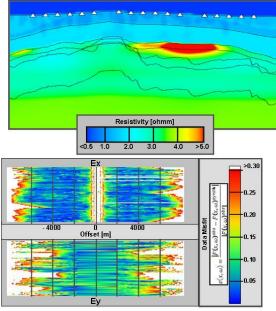

Figure 6: Constrained anisotropic 3D inversion result (vertical resistivity) for the full 3D data set (top) and the resulting data misfit for the Ex and Ey component of the electric field (bottom)

Conclusions

CSEM data was acquired in a deepwater frontier area in Southeast Asia to provide input in a portfolio ranking process and as a risk mitigation tool. A tight 3D grid was chosen to give higher confidence for the interpretation as well as to address uncertainties with respect to the target geometry. The resistivity distribution in the subsurface was then recovered by using multiple unconstrained 3D inversion runs.

The inversion test revealed the importance of using not only the full 3D data set in form of inline and azimuth data, but also the importance of acknowledging the full complexity of the subsurface. When anisotropy is accounted for, significant improvements in the data fit for the azimuthal data was obtained. In addition, not taking anisotropy into account materially impacted the recovered resistivity distribution and the interpretation of the CSEM data. Figure 7 summarizes the resulting difference between an isotropic and anisotropic inversion.

The interpretation of the unconstrained inversion result yielded two alternative models to explain the data, one of the models with a resistivity expression more akin to a

reservoir while the other showed a resistivity distribution, comparable to a thicker sediment sequence with increased resistivities. The results of the constrained 3D inversion were more supportive of a resistivity distribution with a reservoir character.

With respect to the hydrocarbon charge of the initial target, the CSEM data only supported substantial hydrocarbon charge in about one-third of the original designated target area (Figure 8). This reduced the potential of the prospect significantly.
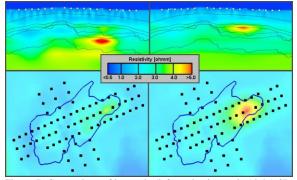

Figure 7: Comparison of isotropic (left) and anisotropic (right) 3D inversion result for inline and azimuthal data combined. Bottom row shows resistivity distribution at target level, top row, cross - section through the resistivity volume along central SW - NE line.
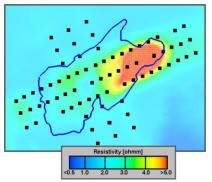

Figure 8: Size of the resistivity anomaly at target level for the constrained anisotropic 3D inversion result versus the original prospect outline.

Acknowledgement

EDITED REFERENCES

Note: This reference list is a copy-edited version of the reference list submitted by the author. Reference lists for the 2010 SEG Technical Program Expanded Abstracts have been copy edited so that references provided with the online metadata for each paper will achieve a high degree of linking to cited sources that appear on the Web.

REFERENCES

Eidesmo, T., S. Ellingsrud, L. M. MacGregor, S. Constable, M. C. Sinha, S. Johansen, F. N. Kong, and H. Westerdahl, 2002, Sea bed logging (SBL), a new method for remote and direct identification of hydrocarbon filled layers in deepwater areas: First Break, **20**, 144–152.

Lu, X., and C. Xia, 2007, Understanding Anisotropy in Marine CSEM Data: 77th Annual International Meeting, SEG, Expanded Abstracts, 633-637

Morten, J. P., and A. K. Bjorke, 2009, Importance of Azimuth Data for 3D Inversion of Marine CSEM Scanning Data: 71st EAGE Conference & Exhiition, Expanded Abstracts

Storen, T., J. J. Zach, and F. Maoo, (2008), Gradient Calculations for 3D Inversion of CSEM data using a fast finite-difference time-domain modelling code: 70th Conference & Exhibition, EAGE, Expanded Abstracts

Zach, J. J., and M. A. Frenkel, 2009, 3D Inversion- Based Interpretation of Marine CSEM Data: Offshore Technology Conference, Houston, Expanded Abstracts